Journal of Astronomical Telescopes, Instruments, and Systems

AstronomicalTelescopes.SPIEDigitalLibrary.org

Study on the application of the free-vibration modes of an annular mirror in the active optics system

Hairen Wang
Ming Liang
Dazhi Yao
Yingxi Zuo
Xianzhong Zheng
Ji Yang

SPIE.

Hairen Wang, Ming Liang, Dazhi Yao, Yingxi Zuo, Xianzhong Zheng, Ji Yang, "Study on the application of the free-vibration modes of an annular mirror in the active optics system," *J. Astron. Telesc. Instrum. Syst.* **6**(1), 019002 (2020), doi: 10.1117/1.JATIS.6.1.019002

Study on the application of the free-vibration modes of an annular mirror in the active optics system

Hairen Wang,[a,b,c,*] Ming Liang,[a] Dazhi Yao,[a] Yingxi Zuo,[a,b] Xianzhong Zheng,[a,b] and Ji Yang[a,b]

[a]Chinese Academy of Sciences, Purple Mountain Observatory, Nanjing, China
[b]Chinese Academy of Sciences, Key Laboratory for Radio Astronomy, Nanjing, China
[c]University of Science and Technology of China, School of Astronomy and Space Science, Hefei, China

Abstract. The free-vibration modes of an annular mirror (FVMAM), derived from the thin plate theory and reflecting the intrinsic characteristics of the physical phenomenon of resonance, have been applied to compensate the aberrations of the active optics system. As an application example, the compensations of some low-order aberrations of the 2.5-m Wide-Field Survey Telescope with the FVMAM have been presented. In addition, a quantitative comparative study of the aberration corrections between the FVMAM and the annular Zernike polynomials has been carried out. The results have shown that the FVMAM are more effective to correct the aberrations. [DOI: 10.1117/1.JATIS.6.1.019002]

Keywords: optical aberrations; free-vibration modes; annular Zernike polynomials; active optics.

Paper 19124 received Dec. 6, 2019; accepted for publication Feb. 26, 2020; published online Mar. 19, 2020.

1 Introduction

The renowned Zernike polynomials, first proposed by Zernike,[1] are widely used to represent the optics aberrations in many optics systems. However, the research results have suggested that the Zernike polynomials work inefficiently in the dynamic range of the aberration corrections of the active optics and the adaptive optics.[2] The task of the active optics systems is to correct the optics aberrations in an effective way.[3] This implies that a good method for correcting the aberrations is to remove the residual errors with minimum loads and the least computing resource. In our previous work,[4] the free-vibration modes of an annular mirror (FVMAM) have been proposed to replace the annular Zernike polynomials. The results have shown that the mode shapes of the FVMAM resemble those of the annular Zernike polynomials, and there is almost a one-to-one match between each mode of the FVMAM and each mode of annular Zernike polynomials. Moreover, the qualitative results have shown that the FVMAM is more likely to perform more efficiently in the aberration corrections of the active optics and the adaptive optics. To verify this, we present a quantitative comparative study of the aberration corrections between the FVMAM and the annular Zernike polynomials.

2 Mathematical Formulation

2.1 *Mathematical Formulation of the FVMAM*

In our previous work,[4] the FVMAM is stemmed from a thin annular plate. An annular mirror made of a glass annular plate is shown in Fig. 1. The thickness of the annular mirror is denoted by $2h$. The outer and the inner diameters of the annular mirror are denoted by $2b$ and $2a$, respectively. The edges of the outer surface $r = b$ and the inner surface $r = a$ are free. This means the

*Address all correspondence to Hairen Wang, E-mail: hairenwang@pmo.ac.cn

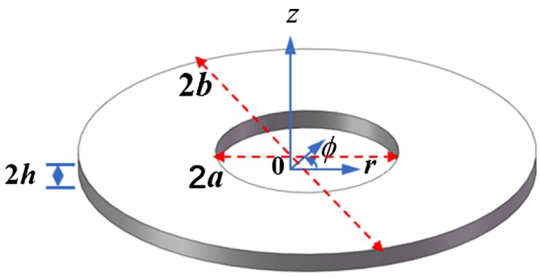

Fig. 1 The configuration of an annular plate.

following modes of the plate are derived from the free vibration. Since the detailed derivation of the FVMAM had been presented in the previous work,[4] here the three-dimensional formulas of the FVMAM are given directly. An arbitrary wave-front error $U(r,\phi)$ can be expanded with the infinite basis terms of the FVMAM:

$$U(r,\phi)=\sum_{n=0}^{\infty}\sum_{m=1}^{\infty}c_{nm}u_{nm}(r)\cos(n\phi), \tag{1}$$

in which the $u_{nm}(r)\cos(n\phi)$ denotes the orthonormal basis terms of the FVMAM, m denotes the order, n denotes the symmetry, and c_{nm} denotes the coefficient of the modes of the FVMAM. Here

$$u_{mn}(r)=K_{nm}\overline{u}_{nm}(r), \tag{2}$$

where

$$K_{nm}=\sqrt{(b^2-a^2)/\left(\eta\int_a^b\overline{w}_{nm}(r)\mathrm{d}r\right)},\quad \eta=\begin{cases}2 & n=0\\ 1 & n>0\end{cases}, \tag{3}$$

$$\overline{u}_{mn}(r)=H_{1,n}J_n(\lambda_m r)+H_{2,n}Y_n(\lambda_m r)+H_{3,n}I_n(\lambda_m r)+H_{4,n}K_n(\lambda_m r), \tag{4}$$

where $J_n(\lambda_m r)$, $Y_n(\lambda_m r)$, $I_n(\lambda_m r)$, and $K_n(\lambda_m r)$ are the n'th-order Bessel function of the first kind with argument $\lambda_m r$, the n'th-order Bessel function of the second kind with the argument $\lambda_m r$, the n'th-order modified Bessel function of the first kind with the argument $\lambda_m r$, and the n'th-order modified Bessel function of the second kind with the argument $\lambda_m r$, respectively. The four unknowns, $H_{1,n}$ to $H_{4,n}$, could be determined by the boundary conditions. Here, λ_m is a function of the material parameters, geometric parameters, and natural frequencies of the annular mirror. (For more details see our previous work.[4])

2.2 *Aberration Compensation Algorithm*

To be easy for a reader to understand, here the brief introduction of the aberration compensation algorithm has been presented. As an application example, the compensations of some low-order aberrations of the 2.5-m Wide-Field Survey Telescope (WFST) with the FVMAM will be presented. The WFST, which will use an advanced active optics control system, has a unique primary focus with a 7-lens corrector system. It provides not only the best image quality over a wide spectrum range from UV to infrared but also over a 3-deg wide field of view. Figure 2 shows the conceptual design model of WFST.[5] The primary mirror of the WFST is supported by 54 pneumatic actuators (see Fig. 3), which are used to adjust the deformation shape of the reflective surface of the primary mirror to compensate the optical aberrations.

The task of the active optics systems is to correct the optics aberrations in an effective way, and a good method for correcting the aberrations is to remove the residual error with minimum loads and the least computing resource.[3] Therefore, the aberration compensation can be served as a general optimization problem, which can be expressed as[5–7]

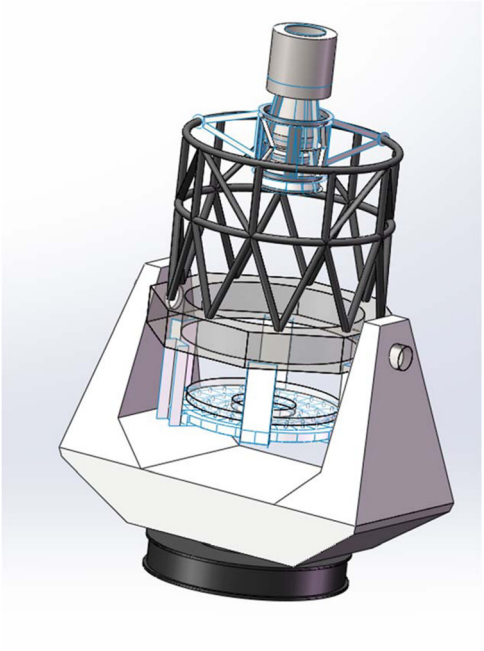

Fig. 2 The conceptual design model of WFST.

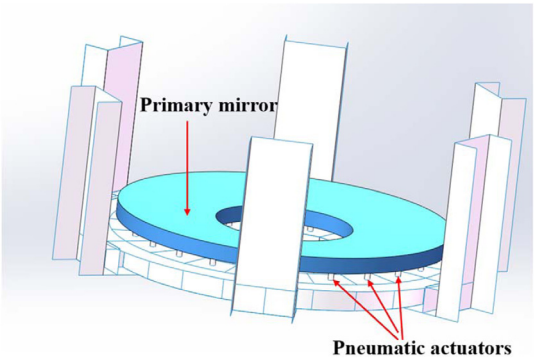

Fig. 3 The support system of primary mirror of WFST.

$$\begin{aligned}
&\Omega = \min\ \Omega(\gamma) \quad \xi = [\xi_1, \xi_2, \ldots, \xi_m] \\
&\text{s.t. } \xi_i^L \le \xi_i \le \xi_i^U \quad (i = 1,2,3,\ldots,m) \\
&\vartheta_j^L \le \vartheta_j(\gamma) \le \vartheta_j^U \quad (j = 1,2,3,\ldots,n_1) \\
&h_j^L \le h_j(\gamma) \le h_j^U \quad (j = 1,2,3,\ldots,n_2) \\
&w_j^L \le w_j(\gamma) \le w_j^U \quad (j = 1,2,3,\ldots,n_3),
\end{aligned} \tag{5}$$

in which Ω is the objective function, and ξ denotes the design variable. The terms ϑ, h, and w are the state variables. Here ξ_i^U, ϑ_j^U, h_j^U, and w_j^U are the upper limits of ξ, ϑ, h, and w, respectively, and ξ_i^L, ϑ_j^L, h_j^L, and w_j^L are their lower limits. The terms m, n_1, n_2, and n_3 are the numbers of ξ, ϑ, h, and w, respectively.[7] Here the hybrid optimization algorithm[5,7] will be applied.

The damped least squares method, proposed by Levenberg and Marquardt, is also named Levenberg–Marquardt algorithm.[8] The corrective forces $\{f\}_s$ of the primary mirror can be calculated with the damped least squares method:[9]

$$\{f\}_s = -([\mathbf{C}]_{r\times s}^{\mathrm{T}}[\mathbf{C}]_{r\times s} + \mathrm{p}[\mathbf{I}]_{s\times s})^{-1}[\mathbf{C}]_{r\times s}^{\mathrm{T}}\{\delta\}_r, \tag{6}$$

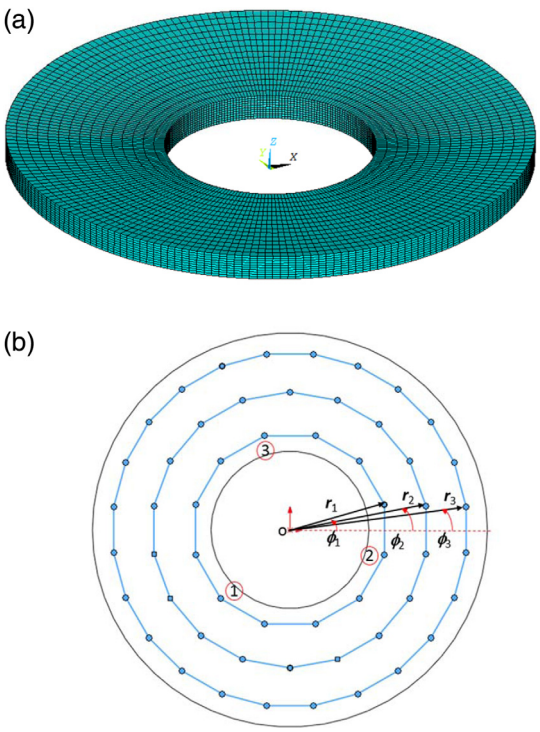

Fig. 4 The FEM of the annular primary mirror of the WFST. (a) The mesh of the FEM. (b) The 54 axial supports points of the primary mirror of the WFST.

where $\{f\}_s$, $\{\delta\}_r$, $[\mathbf{C}]_{r\times s}$, $[\mathbf{I}]$, and p denote an s-dimensional vector of the corrective forces of the support points of the annular mirror, an r-dimensional vector of the displacements of the reflective surface nodes of the annular mirror, a compliance matrix, the unit matrix, and the damping factor, respectively. In this paper, $s = 54$ [see Figs. 3 and 4(b)]. Here p will serve as a design variable in the optimization algorithm. After the optimization, we can obtain the best value of p. In Eq. (6), the value of p includes two components: the linear component and nonlinear component. To separate the linear component from p, a linear scale factor is introduced, as shown in the following equation:

$$\{f^S\} = \kappa\{f\}. \tag{7}$$

In this paper, both κ and p act as two design variables (the optimization factors) during the simulation of the aberration compensation of the active optics. The corrective forces vector $\{f^S\}$ is used as the corrective forces input to be loaded to the 54 supporting points of the primary mirror. The displacement vector $\{\Delta\}$ of the reflective surface, produced by $\{f^S\}$, should be equal to $-\{\delta\}$ in an ideal state but not in practice. Thus, the residual displacement can be obtained as follows:

$$\{w_i\} = \{\delta_i\} + \{\Delta_i\}, \tag{8}$$

where i denotes the i'th node of the reflective surface of the annular mirror. The paraboloidal shape surface meets the following equation[10] provided that the paraboloidal shape of the primary mirror has on any residual displacements:

$$X^2 + Y^2 = 4\Gamma(Z + c), \tag{9}$$

in which Γ and c are the focal length and the vertex z coordinate, respectively. Provided that there are any residual displacements, the reflective surface of the new status meets the equation as follows:

$$X_1^2 + X_1^2 = 4\Gamma(Z_1 + c), \tag{10}$$

where c, which is fixed, is equal to that of Eq. (9). For every node of a reflective surface, the direction cosines of the reflective surface normal can be written as

$$\begin{aligned} 2\cos\varphi_1 &= -\frac{X_i}{\sqrt{\Gamma(\Gamma+Z_i+c)}}, \\ 2\cos\varphi_2 &= -\frac{Y_i}{\sqrt{\Gamma(\Gamma+Z_i+c)}}, \\ 2\cos\varphi_3 &= -\frac{2\Gamma}{\sqrt{\Gamma(\Gamma+Z_i+c)}}. \end{aligned} \tag{11}$$

The displacement of the reflective surface node i is denoted with (u_i, v_i, w_i), and the distance to this best-fitted paraboloid is denoted with σ_i, we can obtain[10]

$$X-(X_i+u_i)=\pm\sigma_i\cos\varphi_1, \quad Y-(Y_i+v_i)=\pm\sigma_i\cos\varphi_2, \quad Z-(Z_i+w_i)=\pm\sigma_i\cos\varphi_3. \tag{12}$$

We can get the geometrical *RMS* distance surface error by the following equation:[10]

$$RMS_g=\sqrt{\frac{1}{r}\sum_{i=1}^{r}\sigma_i^2}. \tag{13}$$

Further, we can acquire the effective residual surface error (the residual half path length error) as follows:[10]

$$RMS_e=\sqrt{\frac{1}{r}\sum_{i=1}^{r}s_i^2} \quad s_i=\sigma_i\cos\psi_i, \tag{14}$$

where ψ is the angle between the surface normal and the reflective surface axis. According to Eqs. (13) and (14), here RMS_{e} is set as the objective function, RMS_{g} is set as the state variable, and p and κ are set as two design variables. Therefore, we can obtain

$$\Omega=RMS_e=\sqrt{\frac{1}{r}\sum_{i=1}^{r}s_i^2} \quad [\xi_1,\xi_2,\cdots,\xi_m]=[p,\kappa] \quad \vartheta=RMS_g=\sqrt{\frac{1}{r}\sum_{i=1}^{r}\sigma_i^2}. \tag{15}$$

In this paper, the hybrid optimization algorithm, proposed by us in previous works,[5,7] has been applied. The hybrid optimization algorithm exploits the complementary merits of both the zero- and first-order optimizations, with the former in global scale and the latter in small scale. Here the convergence criteria are the tolerance errors of p, κ, RMS_{g}, and RMS_{e}, which are constants of 1×10^{-18}, 1×10^{-7}, 1×10^{-18}, and 1×10^{-18}, respectively. In this paper, 55 is also set as the maximum of iteration in each optimization process, but the maximum is usually much less than 55 with the hybrid optimization algorithm providing a fast convergence with a high precision.

3 Numerical Results and Discussion

To illustrate the effectiveness of the FVMAM, we present some numerical results in this section. In following the calculations, we use the compensations of some low-order aberrations of the primary mirror of 2.5-m WFST as the application examples. In all of the following calculations, we choose $2a=1000$ mm, $2b=2500$ mm, and $2h=120$ mm, unless stated otherwise. The material of the mirror is Cer-Vit material, whose mass density, Poisson's ration, and Young's modulus are $\rho=2530\ \mathrm{kg\,m^{-3}}$, $\nu=0.24$, and $E_{\mathrm{m}}=91$ GPa, respectively.[10] Figure 4(a) shows the finite element model (FEM) of the primary mirror of the WFST. Figure 4(b) shows the axial support design of the primary mirror, which has 54 supporting points (pneumatic actuators).

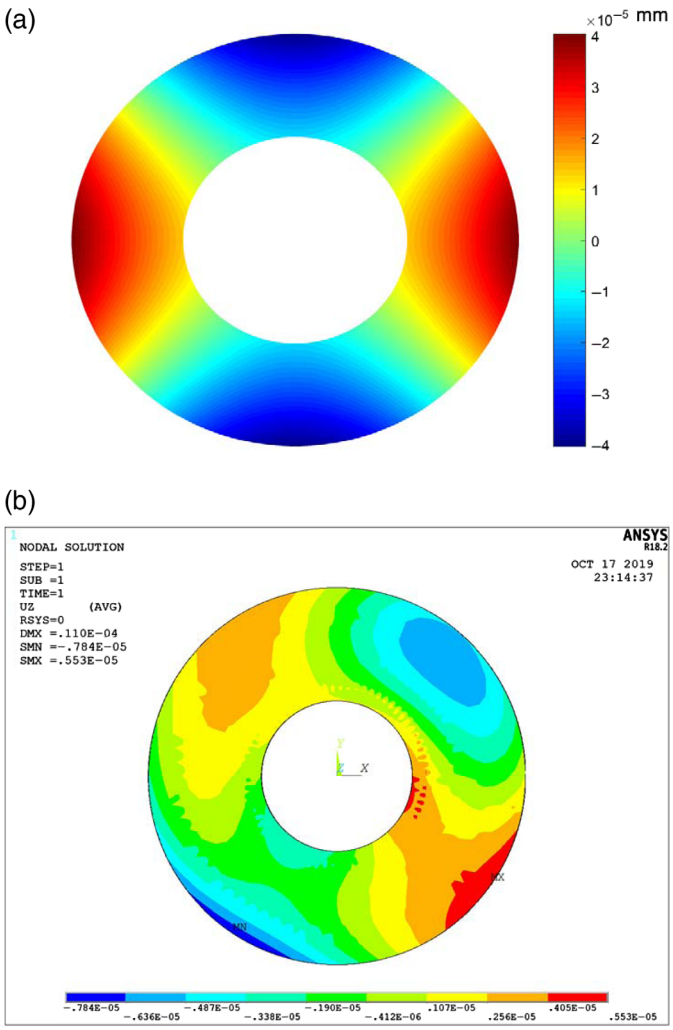

Fig. 5 The initial errors and the minimum residual errors. (a) The distribution of the initial errors of $u_{21}(r)\cos 2\phi$. (b) The distribution of the minimum residual errors of $u_{21}(r)\cos 2\phi$ after one time of correction.

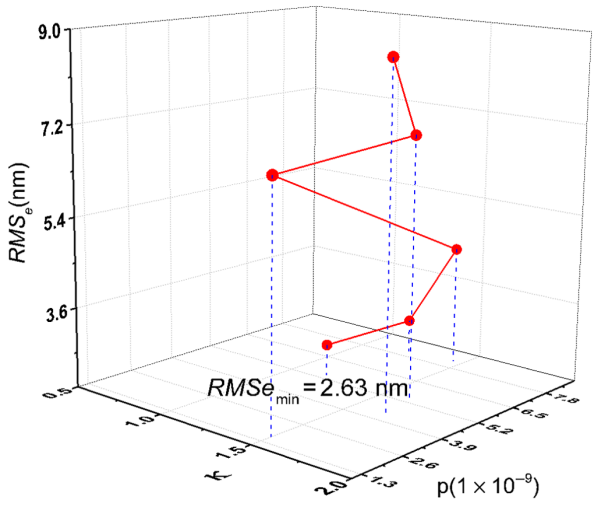

Fig. 6 The relationship between the objective function RMS_e of $u_{21}(r)\cos 2\phi$ and the design variables (p and κ).

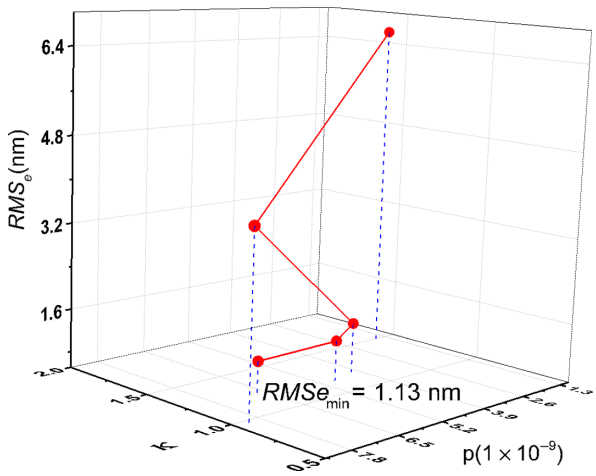

Fig. 7 The relationship between the objective function RMS_e of $u_{21}(r)\sin 2\phi$ and the design variables (p and κ).

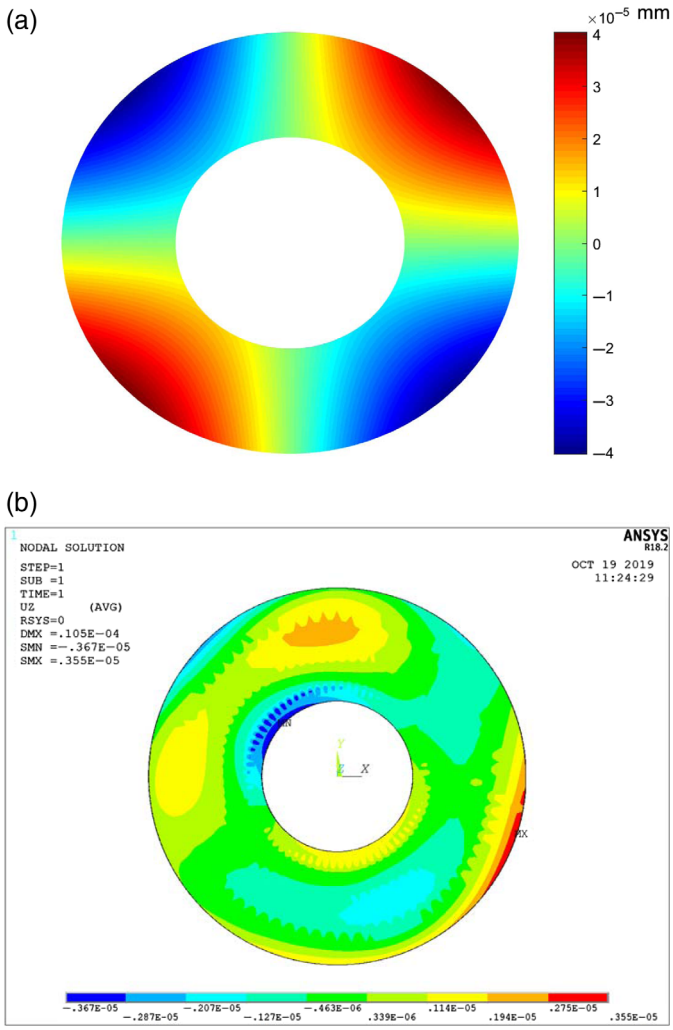

Fig. 8 The initial errors and the minimum residual errors. (a) The distribution of the initial errors of $u_{21}(r)\sin 2\phi$. (b) The distribution of the minimum residual errors of $u_{21}(r)\sin 2\phi$ after one time of correction.

Because the astigmatism aberrations are the commonest aberrations of the active optics telescope, here we choose the correction simulations of four kinds of the astigmatism aberrations, including the $u_{21}(r)\cos 2\phi$, $u_{21}(r)\sin 2\phi$, $u_{31}(r)\cos 3\phi$, and $u_{31}(r)\sin 3\phi$, to illustrate the effectiveness of the FVMAM. These modes can be expressed as follows:

$$\begin{aligned}
u_{21}\cos 2\phi &= K_{21}[H_{1,1}J_1(\lambda_2 r) + H_{2,1}Y_1(\lambda_2 r) + H_{3,1}I_1(\lambda_2 r) + H_{4,1}K_1(\lambda_2 r)]\cos 2\phi,\\
u_{21}\sin 2\phi &= K_{21}[H_{1,1}J_1(\lambda_2 r) + H_{2,1}Y_1(\lambda_2 r) + H_{3,1}I_1(\lambda_2 r) + H_{4,1}K_1(\lambda_2 r)]\sin 2\phi,\\
u_{31}\cos 3\phi &= K_{31}[H_{1,1}J_1(\lambda_3 r) + H_{2,1}Y_1(\lambda_3 r) + H_{3,1}I_1(\lambda_3 r) + H_{4,1}K_1(\lambda_3 r)]\cos 3\phi,\\
u_{31}\sin 3\phi &= K_{31}[H_{1,1}J_1(\lambda_3 r) + H_{2,1}Y_1(\lambda_3 r) + H_{3,1}I_1(\lambda_3 r) + H_{4,1}K_1(\lambda_3 r)]\sin 3\phi. \quad (16)
\end{aligned}$$

In this paper, the initial errors before the optimizing are 30 nm, unless stated otherwise. Figures 5(a), 8(a), 9(a), and 10(a) show the distribution of the initial errors of the four kinds of astigmatism aberrations. Figures 6, 7, 11, and 12 show the relationships between the objective function RMS_e and the design variables (p and κ). Examining at Figs. 6, 7, 11, and 12, it is apparent that the objective function RMS_e is very sensitive to a very slight variation of the design variables (p and κ). Figures 5(b), 8(b), 9(b), and 10(b) show the minimum residual errors of the four kinds of the astigmatism aberrations after one time of the optimizing, and the minimum

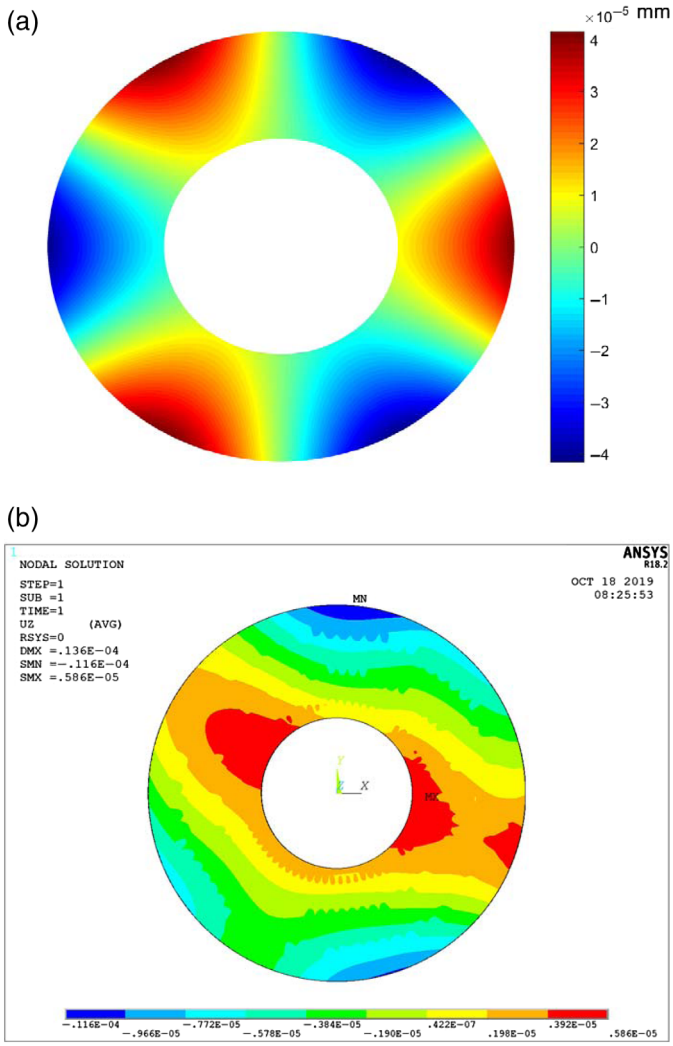

Fig. 9 The initial errors and the minimum residual errors. (a) The distribution of the initial errors of $u_{31}(r)\cos 3\phi$. (b) The distribution of the minimum residual errors of $u_{31}(r)\cos 3\phi$ after one time of correction.

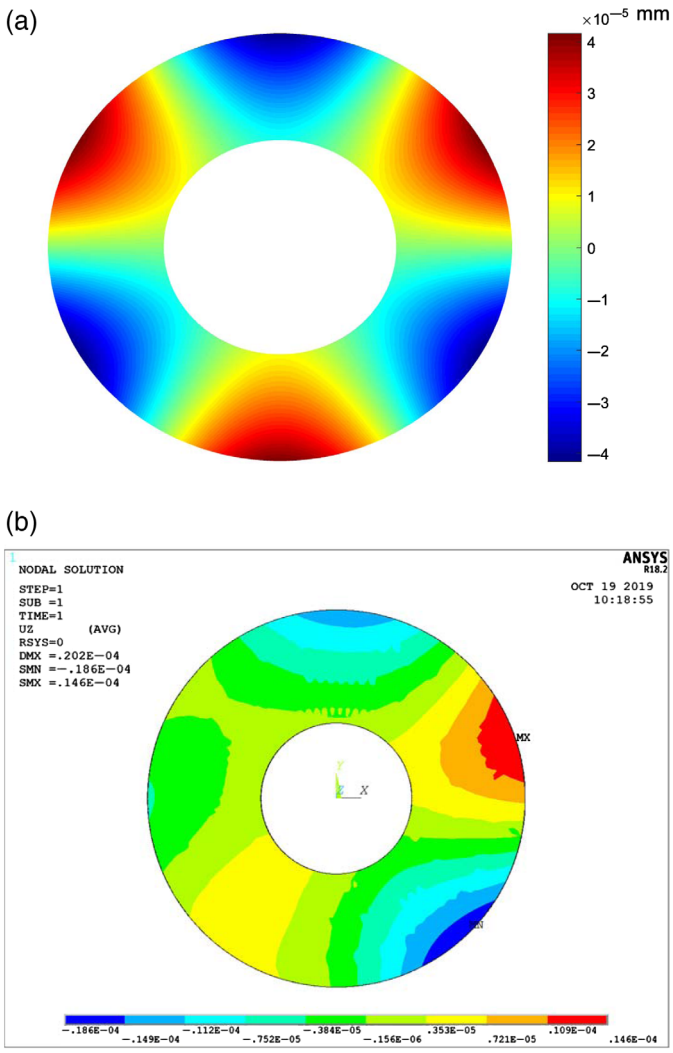

Fig. 10 The initial errors and the minimum residual errors. (a) The distribution of the initial errors of $u_{31}(r)\sin 3\phi$. (b) The distribution of the minimum residual errors of $u_{31}(r)\sin 3\phi$ after one time of correction.

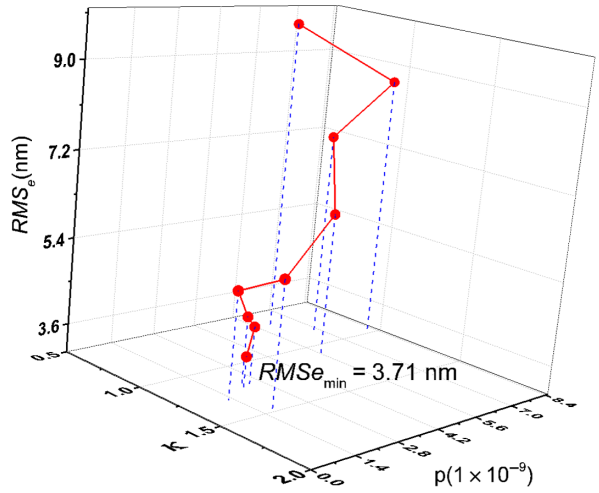

Fig. 11 The relationship between the objective function RMS_e of $u_{31}(r)\cos 3\phi$ and the design variables (p and κ).

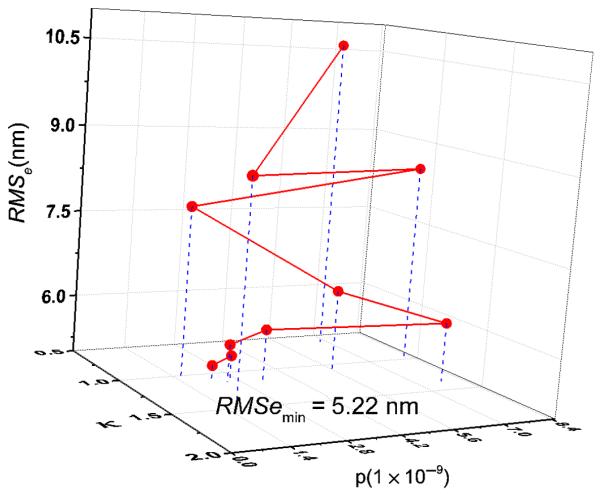

Fig. 12 The relationship between the objective function RMS_e of $u_{31}(r)\sin 3\phi$ and the design variables (p and κ).

Table 1 The detail results of the aberration compensation by the FVMAM.

Error's name	Start errors (nm)	Remaining RMS (nm)	Best damping factor p	Best linear scale factor κ	One time of correction rate (%)	Absolute value of the maximum force (N)	RMS of the forces (N)
$u_{21}\cos 2\phi$	30	2.63	5.41×10^{-9}	1.17	91.23	1.21	0.49
$u_{21}\sin 2\phi$	30	1.13	6.83×10^{-9}	1.20	96.23	1.24	0.47
$u_{31}\cos 3\phi$	30	3.71	1.96×10^{-9}	1.26	87.63	3.74	1.30
$u_{31}\sin 3\phi$	30	5.22	2.21×10^{-9}	1.08	82.60	3.05	1.16

residual errors of $RMS_e = 2.63$, 1.13, 3.71, and 5.22 nm have been stamped on Figs. 6, 7, 11, and 12, respectively. More detailed results of the aberration compensation by the FVMAM have been listed in Table 1. As can be seen from the data in Table 1, 91.23% of the initial errors of $u_{21}(r)\cos 2\phi$, 96.23% of the initial errors of $u_{21}(r)\sin 2\phi$, 87.63% of the initial errors of $u_{31}(r)\cos 3\phi$, and 82.60% of the initial errors of $u_{31}(r)\sin 3\phi$ could be removed after one time of the correction.

The mode shapes of the FVMAM resemble those of the annular Zernike polynomials, and there is almost a one-to-one match between each mode of the FVMAM and each mode of annular Zernike polynomials. Here Z5, Z6, Z9, and Z10, which denote the annular Zernike, correspond to $u_{21}(r)\cos 2\phi$, $u_{21}(r)\sin 2\phi$, $u_{31}(r)\cos 3\phi$, and $u_{31}(r)\sin 3\phi$, respectively (see our previous work[4]). Here Z5, Z6, Z9, and Z10 can be expressed as follows:

$$
\begin{aligned}
Z5 &= \frac{\sqrt{6}r^2\cos 2\phi}{\sqrt{\varsigma^4+\varsigma^2+1}},\\
Z6 &= \frac{\sqrt{6}r^2\sin 2\phi}{\sqrt{\varsigma^4+\varsigma^2+1}},\\
Z9 &= \frac{2\sqrt{2}r^3\cos 3\phi}{\sqrt{\varsigma^6+\varsigma^4+\varsigma^2+1}},\\
Z10 &= \frac{2\sqrt{2}r^3\sin 3\phi}{\sqrt{\varsigma^6+\varsigma^4+\varsigma^2+1}}.
\end{aligned}
\tag{17}
$$

Table 2 The results of the aberration compensation by the annular Zernike polynomials.

Error's name	Start errors (nm)	Remaining RMS (nm)	Best damping factor p	Best linear scale factor κ	One time of correction rate (%)	Absolute value of the maximum force (N)	RMS of the forces (N)
Z5	30	3.24	1.49×10^{-9}	1.14	89.20	4.93	1.74
Z6	30	2.51	1.08×10^{-9}	1.17	91.63	15.12	4.53
Z9	30	6.99	2.00×10^{-9}	1.32	76.70	6.67	2.12
Z10	30	9.61	5.31×10^{-9}	1.47	67.96	3.65	1.68

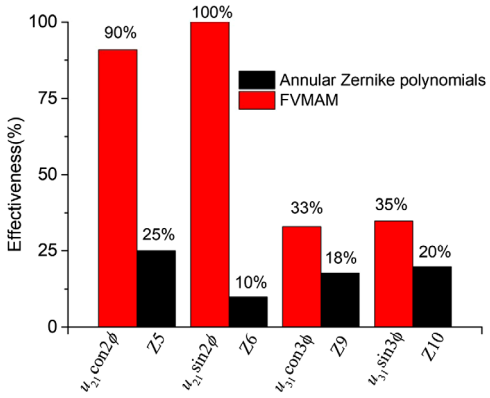

Fig. 13 Comparison the FVMAM and annular Zernike polynomials on effectiveness.

where $\varsigma = a/b$. To demonstrate the efficiency of the FVMAM, a comparative study of the FVMAM and the annular Zernike polynomials is presented. Other being equal (FEA model, etc.), Z5, Z6, Z9, and Z10 are used separately to validate $u_{21}(r)\cos 2\phi$, $u_{21}(r)\sin 2\phi$, $u_{31}(r)\cos 3\phi$, and $u_{31}(r)\sin 3\phi$ quantitatively. As can be seen from the data in Table 2, 89.20% of the initial errors of Z5, 91.63% of the initial errors of Z6, 76.70% of the initial errors of Z9, and 67.96% of the initial errors of Z10 could be removed after one time of correction. The results suggest that the residual errors, after a compensation by the FVMAM, are much better than those of the annular Zernike polynomials (see Tables 1 and 2). Moreover, lower magnitude of correction forces and smaller magnitude of the RMS of correction forces are required with using the FVMAM to compensate the aberrations. In other words, there are two benefits of using FVMAM: (a) lower magnitude of correction force required, which could allow the use of actuators with smaller range and better resolution/repeatability, resulting in a reduction of random force errors that limit the quality of the correction; (b) reduced print-through of high-spatial-frequency bumps on the mirror surface, which spread light widely in the image. Here, comparing the FVMAM and annular Zernike polynomials on effectiveness is also presented (see Fig. 13). The effectiveness metric of each mode, which is defined as dividing the *RMS* surface change by the corresponding *RMS* of the actuator forces, refers to the approach for comparing correction modes, which was proposed by Dr. Jerry Nelson for the Thirty Meter Telescope. In this paper, this metric is highest for $u_{21}(r)\sin 2\phi$, whose effectiveness serves as the criterion. From Fig. 13, it is observed that the effectiveness of each mode of the FVMAM is much larger than that of the matched mode of annular Zernike polynomials.

4 Summary

The goal of this paper is to present an effective way for the aberration compensation of the active optics. The FVMAM, derived from the elasticity theory, reflecting the natural properties of the physical phenomenon of the resonance, are applied in the diffraction theory of the optical

aberrations. Moreover, a quantitative comparative study of the aberration corrections between the FVMAM and the annular Zernike polynomials has been presented. The main conclusion to be drawn from the results of the study is that FVMAM are more effective to correct the aberrations.

Acknowledgments

This work was supported by the Key Research Program of the Chinese Academy of Sciences (CAS)(Grant No. ZDBS-LY-SLH019), the National Natural Science Foundation of China (Grant Nos. 11873100, 11403109, and 11773084), and the Youth Innovation Promotion Association CAS (Grant No. 2019315). This work was also supported by 2.5-m Wide-Field Survey Telescope (WFST) Project of China, which has been started. The authors would like to thank Yuan Qian and Jingquan Cheng for providing the conceptual design model of WFST. The authors also would like to thank anonymous reviewers for offering many constructive suggestions for the paper.

References

1. F. Zernike, "Diffraction theory of the cut procedure and its improved form, the phase contrast method," *Physica* **1**(689–704), 56 (1934).
2. N. Hubin and L. Noethe, "Active optics, adaptive optics, and laser guide stars," *Science* **262**(5138), 1390–1394 (1993).
3. L. Noethe, "Use of minimum-energy modes for modal-active optics corrections of thin meniscus mirrors," *J. Mod. Opt.* **38**(6), 1043–1066 (1991).
4. H. Wang et al., "Free-vibration modes of an annular mirror for the optical aberration representation," *J. Astron. Telesc. Instrum. Syst.* **5**(2), 024002 (2019).
5. H. Wang et al., "Hybrid optimization methodology of variable densities Mesh model for the axial supporting design of wide-field survey telescope," *Opt. Eng.* **55**(3), 035105 (2016).
6. P. W. Christensen and A. Klarbring, *An Introduction to Structural Optimization*, Springer Science & Business Media, Dordrecht (2008).
7. H. Wang et al., "Multi-variable H-β optimization approach for the lateral support design of a Wide Field Survey Telescope," *Appl. Opt.* **55**(31), 8763–8769 (2016).
8. J. J. Moré, "The Levenberg–Marquardt algorithm: implementation and theory," in *Numerical Analysis*, G. A. Watson, pp. 105–116, Springer, Berlin, Heidelberg (1978).
9. Q. Hu and Q. Yao, *The Design of Astronomical Telescope*, Tsinghua University Press, Beijing (2013).
10. J. Cheng, *The Principles of Astronomical Telescope Design*, Springer, New York (2010).

Hairen Wang received his ME degree in physics in 2009 and his PhD in mechanics in 2013 from Huazhong University of Science and Technology (HUST), Wuhan, China. He is currently an associate professor at Purple Mountain Observatory, Chinese Academy of Sciences. Now he is taking part in the 2.5-m Wide-Field Survey Telescope (WFST) Project of China, which has been started. His research interests include adaptive optics system, active optics system, deformable mirror fabrication and design, and telescope's structural mechanics and its thermal control system. He is one of the peer reviewers for *Optics Express*; *Journal of Astronomical Telescopes, Instruments, and Systems*; *Smart Materials and Structures*; *IEEE Transactions on Ultrasonics, Ferroelectrics, and Frequency Control; Applied Optics*; *Journal of Industrial and Engineering Chemistry*, and so on.

Biographies of the other authors are not available.